The global circuit capacitor and two new ways of deriving the time constant of the global atmospheric electric circuit

Journal of Atmospheric and Solar–Terrestrial Physics 273 (2025) 106545

Contents lists available at ScienceDirect

Journal of Atmospheric and Solar-Terrestrial Physics

journal homepage: www.elsevier.com/locate/jastp

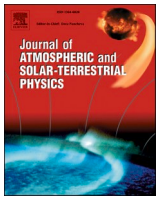

Research Paper

The global circuit capacitor and two new ways of deriving the time constant of the global atmospheric electric circuit

Michael J. Rycroft [a], Alexander P. Nickolaenko [b], R. Giles Harrison [c,*], Anna Odzimek [d]

[a] CAESAR Consultancy, 35 Millington Road, Cambridge, CB3 9HW, UK
[b] O.Ya. Usikov Institute for Radiophysics and Electronics of the National Academy of Sciences of Ukraine, 12, Academician Proskura St., Kharkiv, 61085, Ukraine
[c] Department of Meteorology, University of Reading, Earley Gate, Reading, RG6 6ET, UK
[d] Institute of Geophysics, Polish Academy of Sciences, Ksiecia Janusza 64, 01-452, Warsaw, Poland

ARTICLE INFO

Handling Editor: Dora Pancheva

ABSTRACT

Temporal smoothing of the electrical impulses generated by lightning and shower clouds occurs through the global atmospheric electric circuit (GEC); smoothing is quantified by the time constant of the GEC. Two new methods for calculating this time constant are presented. They are based a) on a novel global circuit capacitor model, rather than the Earth-ionosphere capacitor model, and b) on the concept of dielectric relaxation time of near-surface poorly conducting air. The new GEC model considers the contributions of stratus clouds and their changes to the electrical conductivity of the air. Using model a), the time constants for the various regions of the atmosphere, over land and oceans, are obtained and the GEC time constant is found to be ~10 min. This compares very favourably with the time constant derived from recent observations of the effects of sudden volcanic lightning on the GEC. The upper "pseudo-electrode" of the capacitor, the actual value of whose constant potential varies according to the conditions present, is found to be at an altitude of 1.8 km. For model b), the upper pseudo-electrode is placed at the boundary between dielectric and conducting atmospheres, i.e. where the displacement current equals the conduction current. Its altitude is 2.0 km, in the vicinity of stratiform clouds; the GEC time constant is 7.6 min. The vertical profile of air conductivity which best fits both DC GEC and AC (Schumann resonance) considerations is presented. Smoothing from the GEC's time constant provides steady background conditions for stratiform cloud edge charging which may affect their properties in the climate system; the steady conditions are also exploited biologically, e.g., by spiders and their webs. Other connections between atmospheric electricity and various living species are briefly explored.

1. Introduction

In the Golden Jubilee issue of the Journal of Atmospheric and Solar-Terrestrial Physics, Rycroft et al. (2000) reviewed work on the DC global atmospheric electric circuit, conceived by Wilson (1903, 1906, 1921, 1929). Currents in this circuit, powered mainly by thunderstorms, flow up to and in the ionosphere, down through the atmosphere remote from thunderstorms, through the Earth's surface and, via point discharge currents, up to the thunderclouds. They considered how the global circuit might respond to changing solar activity and to climate change. This followed up on the perceptive tutorial paper by Roble and Hays (1979) in Maynard (1979).

Considerable progress has been made in the last twenty years in understanding both the properties and behaviour of the global electric circuit and the physics that lies behind it. Electrified shower clouds are included in models as a generator as well as thunderstorms, and the variability of the GEC on time scales from diurnal to annual is studied (Siingh et al., 2007, 2023; Williams, 2009; Baumgaertner et al., 2013; Williams and Mareev, 2014; Mareev and Volodin, 2014; Lavigne et al., 2017; Ilin et al., 2020; Potdar and Siingh, 2024). The behaviour of the global circuit on shorter time scales, in particularly the circuit relaxation time, has been of interest to explain how the fair weather electric field, $\boldsymbol{E}$, is maintained globally, and how the DC circuit responds to excitations. Some physical links between climate and the global circuit have been investigated in more detail, including the important role played by the time constant (Harrison, 2004; Tinsley, 2008), which makes it particularly worth investigating. The circuit responses and time constants have generally been modelled (Rycroft et al., 2000; Rycroft et al.,

* Corresponding author.
E-mail addresses: michaelrycroft@btinternet.com (M.J. Rycroft), r.g.harrison@reading.ac.uk (R.G. Harrison).

https://doi.org/10.1016/j.jastp.2025.106545
Received 25 November 2024; Received in revised form 6 May 2025; Accepted 17 May 2025
Available online 19 May 2025

2007; Jánsky and Pasko, 2014; Lucas et al., 2015), but a breakthrough has been recently achieved in obtaining direct observational estimates of the time constant (Bór et al., 2023; Rycroft et al., 2024).

An intuitive way of investigating the relaxation time of the GEC is by using an equivalent circuit, i.e. an electrical engineering representation of the circuit. Fig. 5 of Rycroft et al. (2000) showed a schematic diagram of the GEC and an analogue circuit diagram which represents it. It shows that most of the positive charge in the atmosphere resides close to the Earth's surface. The circuit time constant $\tau = RC$ was also shown in the bottom right-hand corner. Here R is the resistance of the entire atmosphere, which is generally taken to be 200 Ω or, sometimes, 250 Ω (see Tinsley and Zhou (2006), Denisenko et al. (2019a, b)), or an intermediate value. Assuming that a uniform leaky dielectric medium (with a permittivity, or dielectric constant, equal to 1.0006) exists between two concentric conducting spheres representing the Earth (of radius R_E) and the ionosphere (at height h above the Earth's surface which is $\ll R_E$), the capacitance of these two spheres is derived by standard electrostatics theory to be

$$C = 4\pi\varepsilon_0 \frac{R_E^2}{h} \tag{1}$$

Rycroft et al. (2000) termed this the capacitance, C, of the "concentric shell of atmosphere between the Earth and the ionosphere", which we can abbreviate as the "Earth-ionosphere capacitor", over one scale height of the atmosphere rather than over the full height of the ionosphere.

Recognising that the atmosphere is inhomogeneous, and because the density of the Earth's neutral atmosphere decreases exponentially with increasing height, with a scale height of H (~7 km), Rycroft et al. (2000) put $h = H$. This leads to $C = 0.65$ F, giving a time constant of 130 s. However, this is not now considered to be correct.

Rycroft et al. (2024) presented new electrical engineering models of the DC global electric circuit which included the effects of low altitude electrified stratus clouds. These models have thunderstorms, electrified shower clouds and volcanic lightning as generators which cause an upward current to the ionosphere of ~1–1.25 kA. The potential of the ionosphere with respect to the Earth's surface is thereby maintained at ~ + 250 kV. For the cloudy (fair weather and semi-fair weather) portions of the atmosphere over 30 % of the Earth's surface, they considered $R = 305$ Ω and $C = 1.05$ F, whose time constant is 320 s.

The downward current density through the atmosphere ($\boldsymbol{J} \sim 2$ pA/m^2) is modelled by Rycroft et al. (2024) via three circuits in parallel with one another. These represent regions of (i) stratus clouds over the relatively polluted land, (ii) stratus clouds over the relatively unpolluted - yet containing more aerosols - oceans, and (iii) cloud-free and fair weather (with higher altitude, e.g., cumulus, clouds) having clean air (Baumgaertner et al., 2014). The proportions of the Earth's surface covered by these three regions are, respectively, about 4 %, 25 % and 70 %. The proportion covered by thunderstorm generators is <0.2 %, which is negligible in this context. The importance of the relation between the downward current density and cloud microphysics has been emphasised by Tinsley (2008, 2022, 2024) and Rycroft et al. (2024); this research area deserves more study.

If the generator voltage were to be suddenly switched off in such a circuit involving a resistor R and capacitor C in parallel, the voltage would decay exponentially with a time constant $\tau = RC$. In that time the voltage falls to 37 % of its original value, in three time constants to 5 %, and in five time constants to less than 1 % of its original value, i.e. to essentially zero.

Rycroft et al. (2024) noted that numerical values for τ ranged from 6.8 to 8.3 min for the different complex circuit models considered. Observing sudden changes in the excitation of the GEC by lightning from the 21 and May 22, 2011 Grímsvötn volcanic eruption in Iceland, they found that an experimentally determined value for this time constant lay between 7 and 12 min, peaking at 9 min. Bór et al. (2023) found a time constant of ~7–8 min from similar marked changes in volcanic lightning produced by the Hunga Tonga-Hunga Ha'apai eruption on 15 January 2022. These modelled and experimental values are all in good agreement with one another. One may reasonably conclude that the time constant τ is 9 ± 3 min, both theoretically and experimentally.

Here we present an alternative approach to finding the time constant for the GEC which is shown diagrammatically in Fig. 1. The time constant τ is defined in terms of the dielectric relaxation time of the poorly conducting air, which is expressed as

$$\tau = \frac{\varepsilon_0}{\sigma} \tag{2}$$

where ε_0 is the permittivity of free space and σ is the electrical conductivity of the air. Rycroft et al. (2007) presented in their Fig. 2 a model for the vertical profile of electrical conductivity of the air, caused by solar UV and X-radiation, cosmic rays and radioactivity (Kamsali et al., 2011; Golubenko et al., 2020). The conductivity increases from that found at the Earth's surface, where its value is σ_0, up to the ionosphere where it is seven orders of magnitude larger than this. The dielectric relaxation time is also shown in that figure. Clearly, the relaxation time is largest where the conductivity of the air is smallest. The electrical resistance of a vertical column of air (e.g., Harrison, 2005; Rycroft et al., 2008) is mainly determined by the conductivity of the air where it is smallest, namely at, and just above, the Earth's surface. It is therefore the electrical conductivity of the surface air that determines the time constant of the global electric circuit.

In this paper we use an optimal electrical engineering representation of the GEC to introduce the concept of the global circuit capacitor, and consider at what height its upper pseudo-electrode is for two new models of the GEC. We aim to find an optimum vertical profile of air conductivity which agrees with observations of both the DC and AC GECs, and explore some links between atmospheric electricity and different living species.

2. GEC theory

Here we discuss the time constants involved in the circuit diagram shown in Fig. 1b (see also Fig. 4 of Rycroft et al. (2024)). This is a model for the GEC that incorporates.

(i) stratus clouds over land, having higher aerosol concentrations (due to pollution) than over the ocean, which reduces the electrical conductivity of the air,
(ii) stratus clouds over oceans, and
(iii) mid- and high-level clouds in semi-fair weather regions and cloud-free fair weather regions over land, and
(iv) as (iii), but over the oceans.

Here we consider the time constants of these circuits in a different way, using values of the air conductivities, and their relationships with the relaxation times (equation (2) and Fig. 1b)). We consider the non-generator aspects of the circuit from the downward flowing current sections of Fig. 4 in Rycroft et al. (2024), by rearranging the resistances and capacitances into four parallel RC circuits (Fig. 1b)). Circuits 1 and 2 refer to the land and ocean stratus regions, and 3 and 4 to the land and ocean fair weather regions, respectively. They are connected to a pseudo-electrode, i.e. to a conducting plate which everywhere has the same electric potential. Then we replace the dependence on capacitance with a dependence on relaxation time.

To keep matters as simple as possible, we first consider just two parallel RC circuits where the reciprocal of the effective resistance of the combination is given by the sum of the reciprocals of the parallel resistances. The time constant of the combined circuit is therefore

$$\tau = \frac{C_1 + C_2}{\frac{1}{R_1} + \frac{1}{R_2}} = \frac{C_1 + C_2}{\frac{R_2}{R_1 R_2} + \frac{R_1}{R_1 R_2}} = \frac{R_1 R_2 (C_1 + C_2)}{R_1 + R_2} \tag{3}$$

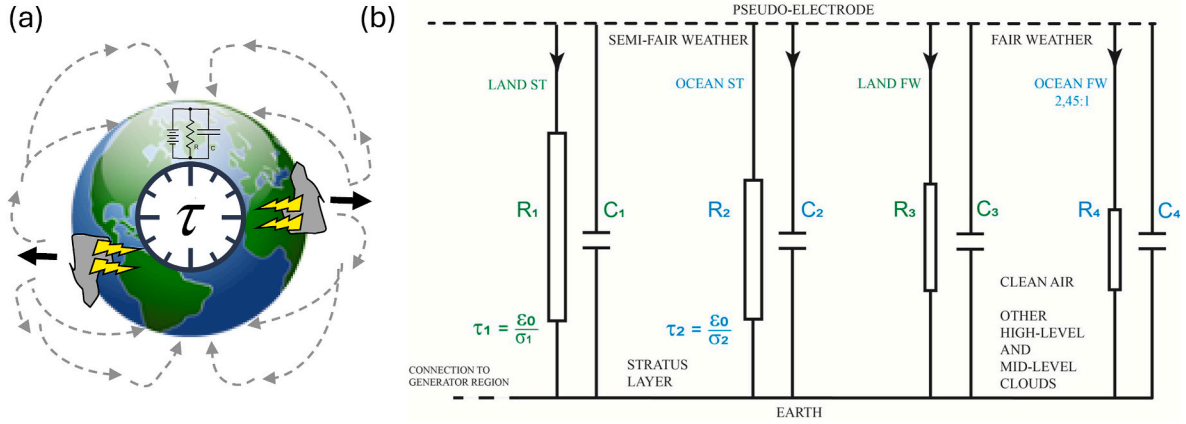

Fig. 1. a). Conceptual representation of the time constant τ of the global atmospheric electric circuit, the dominant voltage generator, namely thunderstorms, causing an upward current (dark arrows) to the ionosphere, and the return currents (dashed arrows) down through the atmosphere at all latitudes and longitudes. b). Circuit representation of the passive part of the lower atmosphere GEC, divided into four regions of land (green) and ocean (blue) semi-fair (ST, stratus layer) and fair weather areas (see Sections 2 and 3), connected to a pseudo-electrode (see text for a definition and discussion). The relationship between the relaxation time τ, the air conductivity σ and the permittivity of free space ε_0 is shown. This circuit is an extension of the lower right-hand part of Fig. 4 of Rycroft et al. (2024), which shows the stratus layer over land and ocean and the fair weather atmosphere, without distinguishing between land and ocean situations.

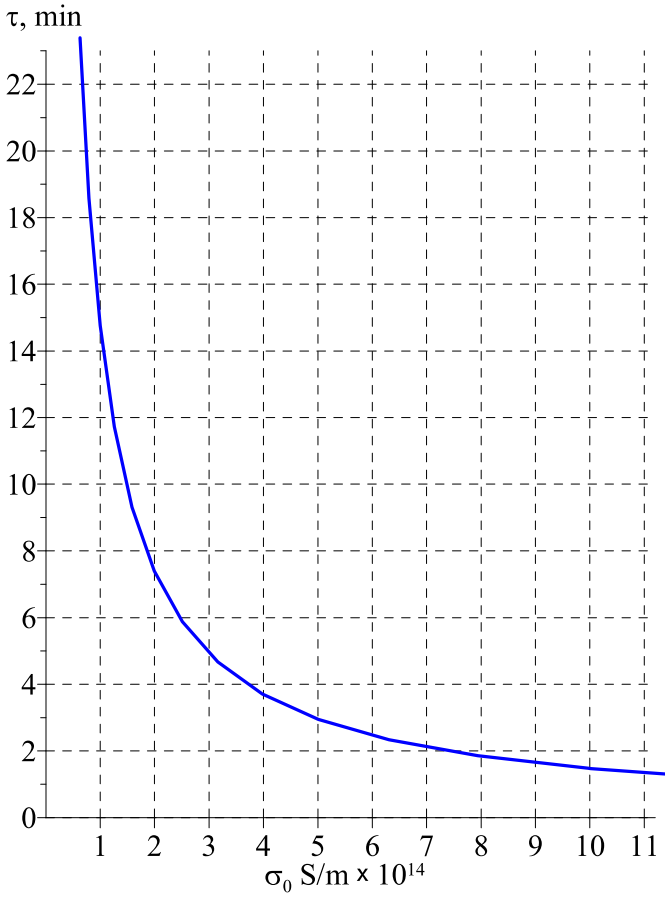

Fig. 2. Variation of the time constant of the global electric circuit, τ, in minutes, with the assumed electrical conductivity of the air at the Earth's surface, σ_0.

Thus,

$$\tau = \frac{\tau_1 R_2}{R_1 + R_2} + \frac{\tau_2 R_1}{R_1 + R_2} \tag{4}$$

Hence, in terms of the conductivity of the air,

$$\tau = \frac{\varepsilon_0}{\sigma} = \frac{\varepsilon_0}{\sigma_1}\frac{R_2}{R_1 + R_2} + \frac{\varepsilon_0}{\sigma_2}\frac{R_1}{R_1 + R_2} \tag{5}$$

where σ_1 and σ_2 are air conductivities under stratus clouds over the land (1) and oceans (2). In the strict definition $\sigma_{1,2}$ would be defined in Eq. (5) by $\sigma_{1,2} = R_{1,2}C_{1,2}/\varepsilon_0$. Instead, we choose representative conductivities in the parallel circuits, and we eliminate the dependence on the capacitance and the height of the pseudo-electrode, noting that the resistances would not change much if this pseudo-electrode were at a slightly different height. We use the values of the conductivities at ground or sea level.

For four RC circuits in parallel, we first consider circuits 1 and 2, and then 3 and 4, and then the two combined circuits 1/2 and 3/4. We obtain a final equation which gives the overall circuit time constant in terms of the time constants of the four separate return circuits weighted by the factors R_n/R, where $n = 1$, 2, 3 or 4.

3. Numerical results

We now put numerical values into these equations. First for equation (2), with $\varepsilon_0 = 8.854 \times 10^{-12}$ (in C/V.m) and σ (in S/m), for which a typical value just above the Earth's surface (subscript 0) is $\sigma_0 = 1.0 \times 10^{-14}$ S/m, from Rycroft et al. (2007) (see also Zhou and Tinsley, 2010), we obtain

$$\tau = 885.4 \text{ s} = 14.76 \text{ minutes} \tag{6}$$

On the other hand, taking $\sigma_0 = 0.759 \times 10^{-14}$ S/m, from Kudintseva et al. (2016), leads to $\tau = 19.45$ min.

Other values of $\tau = \varepsilon_0/\sigma_0$ are plotted in a graph of τ against σ_0 in Fig. 2. This is a rectangular hyperbola, showing the time constant τ, in minutes, plotted against the electrical conductivity of the air just above the Earth's surface σ_0 in S/m x 10^{14}. A rather sharp decrease of τ is evident as σ_0 increases.

We now consider the values of the time constants for the four constituents of the return part of the global circuit, with (i) stratus clouds over land, (ii) stratus clouds over the oceans, and (iii) cloudy semi-fair and fair weather regions over land, and (iv) cloudy semi-fair and fair weather regions over the oceans. For the first pair of regions whose resistances are shown just above the Earth's surface in Fig. 4 of Rycroft et al. (2024), $R_1 = (2980 + 9245 + 2235)\ \Omega = 14460\ \Omega$ and $R_2 = (259 + 1095 + 187)\ \Omega = 1541\ \Omega$, we have, using equation (4) for these two parallel circuits

$$\tau_{12} = 14.76\left[\frac{1541}{16001}\cdot 1.00 + \frac{14460}{16001}\cdot\frac{1.0}{1.6}\right] = 14.76[0.096 + 0.565] =$$

$$14.76 \cdot 0.661 \text{ s} = 9.75 \text{ minutes} \quad (7)$$

Considering that the Earth's surface area is 29 % land and 71 % oceans, so that the ocean surface area is 2.45 times the land surface area, and remembering that the total semi-fair and fair weather resistance to Earth is 305 Ω, but neglecting the different conductivity profiles over land and ocean, shown in Fig. 3 of Rycroft et al. (2024), which would have a smaller effect than do the different resistances, we obtain.

$R_3 = (0.71/0.29)\ R_4 = 2.45\ R_4$ and, using equation (4),

$1/305 = 1/2.45\ R_4 + 1/R_4 = (3.45/2.45)/R_4$,

so that $R_4 = 429$ Ω and $R_3 = 1052$ Ω.

Therefore, using equation (5) again, with $R_3 + R_4 = 1480$ Ω, and $\sigma_3 = \sigma_1$ for land, and $\sigma_4 = \sigma_2$ for oceans,

$$\tau_{34} = 14.76\left[\frac{429}{1480} + \frac{1052}{1480}\cdot\frac{1.0}{1.6}\right] = 14.76[0.290 + 0.444] = 14.76 \cdot 0.734 \text{ s} = 10.82 \text{ minutes} \quad (8)$$

Alternatively, combining regions with the same values of electrical conductivity of the air, with $R_1 + R_3 = 2980 + 1052 = 4032$ Ω,

$$\tau_{13} = 14.76\left[\frac{1052}{15512} + \frac{14460}{15512}\right] = 14.76[0.068 + 0.932] \text{ s} = 14.76 \text{ minutes} \quad (9)$$

which confirms the correctness of the procedure, and

$$\tau_{24} = \frac{14.76}{1.60}\left[\frac{429}{1970} + \frac{1541}{1970}\right] = \frac{14.76}{1.60} \text{ s} = 9.23 \text{ minutes} \quad (10)$$

In order to use equation (3) to combine the two combined regions, we need to calculate the resistance, R_{13}, of R_1 and R_3 in parallel.

$1/R_{13} = 1/14460 + 1/1052 = (0.69 + 9.51)\ 10^{-4} = 1.02 \times 10^{-3}$

so that $R_{13} = 980$ Ω (11)

and $1/R_{24} = 1/1541 + 1/429 = (0.65 + 2.33)\ 10^{-3} = 2.98 \times 10^{-3}$

so that $R_{24} = 336$ Ω. (12)

Hence, using equation (4) with R_{13} replacing R_1 and R_{24} replacing R_2, and with τ_{13} for τ_1 and τ_{24} for τ_2, we obtain the final result for the time constant of the GEC, τ, similarly to equation (7), as

$$\tau_{24} = 14.76\left[\frac{336}{980 + 336} + \frac{980}{1316\cdot 1.60}\right] = 14.76[0.255 + 0.465] =$$

$$14.76 \cdot 0.72 = 10.6 \text{ minutes} \quad (13)$$

Rounding to two significant figures, τ is 11 min.

From Fig. 2, this shows that the global circuit behaves as if the global average value of the electrical conductivity of the surface air was $\sigma_0 = 1.4 \times 10^{-14}$ S/m.

This calculation shows that the more important contribution to the value of the time constant of the global circuit is the air column over the oceans (circuits 2/4) rather than over the land (circuits 1/3), by a factor of 0.517/0.173 = 3.0. This is larger than the aforementioned ocean to land surface area ratio, 2.45.

A limitation of our present study is that, whilst values of E, J and R can be available at a given location and time to within a certain experimental error, globally averaged values are not known with great accuracy. It is even difficult to estimate quantitively what the uncertainties in their estimates might be. We consider that such globally averaged values are correct to one significant figure, but we start by using two significant figures and then rounding appropriately at the end of the calculation.

For example, the air conductivity over land is reduced by a factor of 1.6 from its value over the oceans of 1.6×10^{-14} S/m, i.e. to 1.0×10^{-14} S/m. In this context it is noteworthy that Misaki et al. (1972) reported that the mean observed electrical conductivity of air over the mid-oceans obtained in four different papers ranged from 1.1 to 2.5 × 10^{-14} S/m. Kamra et al. (2001) reported a typical value over the Indian Ocean of 2.0×10^{-14} S/m.

As mentioned earlier, and considering the discussions in, e.g., Zhou and Tinsley (2010) and Denisenko et al. (2019a, b), Section 8, we may take a typical value for the total load resistance of the atmosphere, R, to be 200 Ω, as in Rycroft et al. (2000). Using the value of τ given in equation (13), the capacitance of the Earth-atmosphere capacitor, which we can term the global circuit capacitor, is $\tau/R = 3.06$ F. This is almost

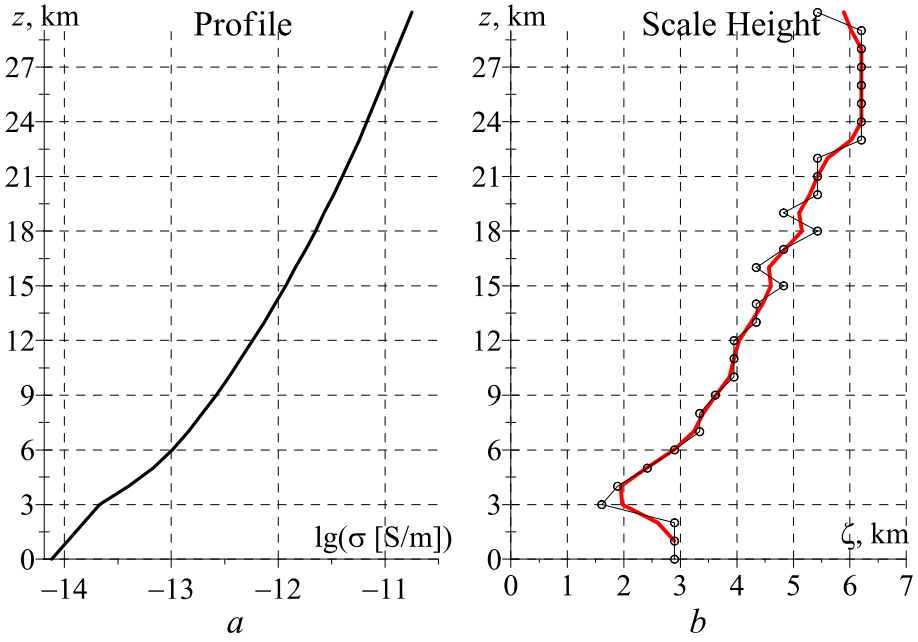

Fig. 3. a) Left: Model profile of the electrical conductivity of the air, σ, in S/m, up to an altitude of $z = 30$ km (from Kudintseva et al., 2018). b) Right: Altitudinal variation of the exponential scale height of the conductivity variation, ζ, in km, up to 30 km. The red curve gives the result of smoothing the $\zeta(h)$ dependence using a triple Hamming window (weights: 0.23; 0.54; 0.23).

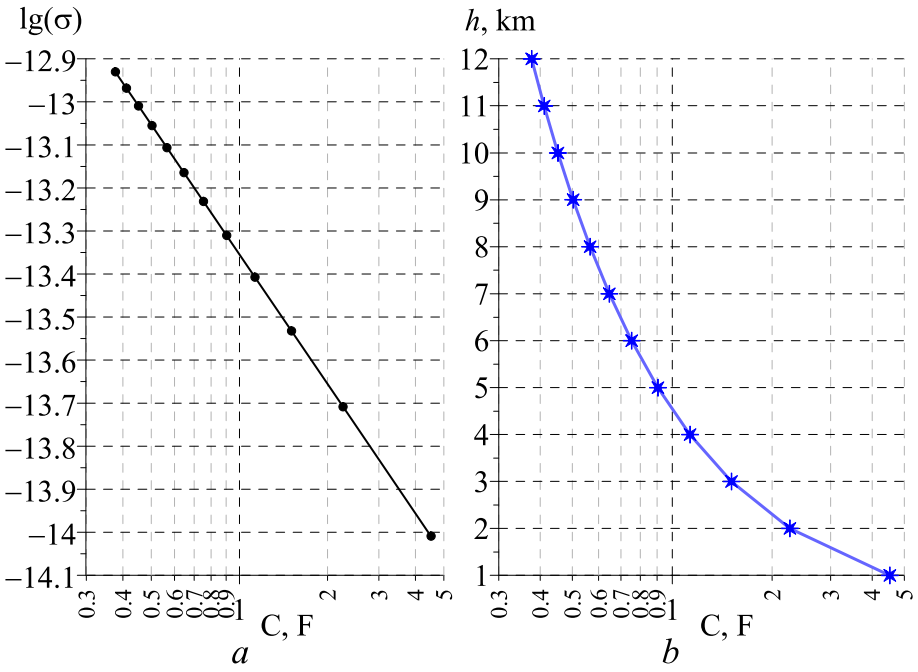

Fig. 4. a) Left. Logarithm of the necessary conductivity of the air at the upper plate versus the capacitance of the global circuit capacitor. b) Right. Height of the upper plate of the capacitor versus the capacitance.

three times the value shown in Fig. 4 of Rycroft et al. (2024) which was prescribed assuming the height of the upper pseudo-electrode of the global circuit capacitor was 3 km. In agreement with the discussions of Haldoupis et al. (2017), this is much lower than the height of the ionosphere.

Using the time constant value given by equation (13) to estimate the height of the pseudo-electrode, in other words the thickness of the capacitance, we find

$$H = \frac{\varepsilon_0 A\, R}{\tau} = \frac{8.85 \cdot 510 \cdot 250}{10.6 \cdot 60}\ \text{m} = 1.77\ \text{km} \tag{14}$$

where A is the Earth's surface area, 510×10^{12} m^2, and R is the total resistance 250 Ω. To two significant figures, H is 1.8 km.

Fig. 3a plots the conductivity profile up to 30 km above the Earth's surface; that profile is the average profile from Kudintseva et al. (2018), which is a further development of the profile introduced by Kudintseva et al. (2016). In this model, the conductivity just above the surface is 0.759×10^{-14} S/m, lower than the value of 1.0×10^{-14} S/m considered here. The scale height of the profile, plotted in Fig. 3b, has the value 2.895 km over the first 3 km. We therefore find that

$$C = \frac{4\pi\varepsilon_0 R_E^2}{2895} = 1.56\ \text{F} \tag{15}$$

When the "pseudo-electrode" (an electrode which does not maintain a constant potential, but whose actual potential varies according to the conditions present) that is the upper plate of the capacitor has a height which is considerably lower than the ionosphere, and when the spatial distribution of charged particles in the capacitor is not uniform between the plates, but is largest close to the lower surface, due to the dielectric inhomogeneity, the capacitor is more accurately described as the *global circuit capacitor*. It was also the subject of investigations of Rycroft et al. (2007) and Rycroft and Odzimek (2010) in connection with studies of upper atmosphere lightning. In these last two works the inhomogeneity of the fair weather region was neglected, however, which affects the time constants obtained in those works.

4. GEC electrodynamics

A stratified atmosphere with a vertically varying conductivity profile is described by the complex dielectric constant

$$\varepsilon(f) = 1 + \frac{i\sigma}{2\pi f \varepsilon_0} \tag{16}$$

with f being the frequency of the electrical signals transferred. The medium should be treated as a dielectric when its imaginary part is much smaller than the real part; it becomes a conductor when the imaginary part substantially exceeds the real part. The boundary between the dielectric and conducting types of medium is therefore found at the level where $\sigma_b = 2\pi f \varepsilon_0$. Physically, this condition means that the displacement current at a given frequency f becomes equal to the conduction current at a particular altitude i.e. that $\varepsilon_0\, d\boldsymbol{E}/dt = \sigma\, \boldsymbol{E}$, where $\boldsymbol{E}$ is an oscillating electric field. Thus, we could argue that the upper capacitor plate should be placed where

$$\sigma_b = 2\pi f \varepsilon_0 = \frac{\varepsilon_0}{\tau}\ . \tag{17}$$

Table 1, columns on the left (1), show the capacitance, C, as given by equation (1), and the boundary conductivity at the upper plate, σ_b, from equation (17) for $R = 200$ Ω against the height of the Earth-atmosphere capacitor, h.

By using data listed in the second and the fourth columns of Table 1, we can construct Fig. 4.

On the left, the abscissa of Fig. 4 shows on a logarithmic scale the capacitance of the spherical cavity between the Earth and the conducting layers of the atmosphere, i.e. the global circuit capacitor. This parameter depends on the distance between the ground and the upper pseudo-electrode of the capacitor. The ordinate in the left panel depicts the $\log(\sigma_b)$ relevant to the "equal current condition" that is traditionally used in the analysis of electrical circuits. Using this condition determines the capacitance and also the height of the upper pseudo-electrode of the capacitor.

Using the data of Table 1 we plot the capacitor height h against $\lg(\sigma_b)$ in Fig. 5. This figure also shows, in red, the conductivity profile from Kudintseva et al. (2018). The idea is to search for the intersection of

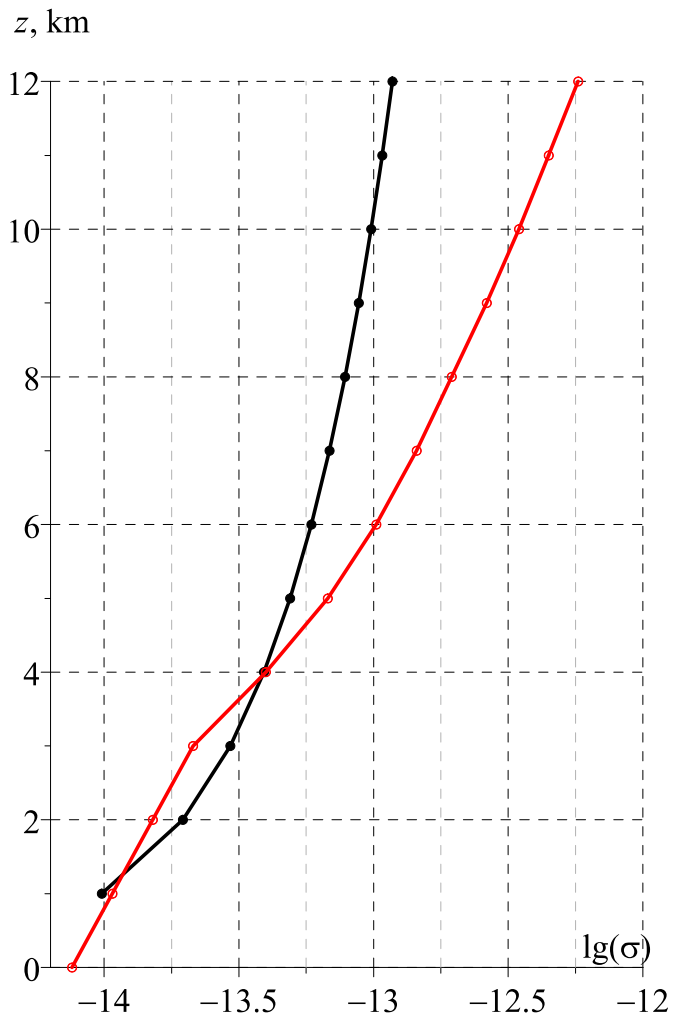

Fig. 5. The black curve shows the capacitor height, h, plotted against $\lg(\sigma_b)$. The red curve shows the air conductivity profile of Kudintseva et al. (2018). The two curves cross at heights between 1.6 and 4 km.

Table 1
Profiles from 1 km up to 12 km of the capacitance of the global circuit capacitor, C, in F, the circuit time constant, τ, in s, and the boundary conductivity, σ_b, between dielectric and conducting behaviours for the atmospheric conductivity profile of Kudintseva et al. (2018), shown as profile 1, and that profile lowered by 0.8 km, shown as profile 2.

h, m	C, F		$\tau = CR$, s		$\sigma_b \cdot 10^{14}$, S/m	
	1	2	1	2	1	2
1000	4.56	4.52	911	904	0.97	0.98
2000	2.28	2.26	456	452	1.94	1.96
3000	1.52	1.51	304	301	2.91	2.94
4000	1.14	1.13	228	226	3.89	3.92
5000	0.91	0.94	182	181	4.86	4.90
6000	0.76	0.75	152	151	5.83	5.88
7000	0.65	0.65	130	129	6.80	6.90
8000	0.57	0.56	114	113	7.77	7.83
9000	0.51	0.50	101	100	8.74	8.81
10000	0.45	0.45	91.1	90.4	9.71	9.79
11000	0.41	0.41	82.9	82.2	10.7	10.8
12000	0.37	0.38	76.0	75.4	11.7	11.8

these two curves. The altitude of this intersection determines the capacitance, C, of the Earth-atmosphere capacitor and hence its time constant, RC. The result is that the height of the upper plate of the capacitor is 3 ± 1 km; the capacitance lies between 1.1 F and 2.3 F. Therefore, the time constant $\tau = RC$ is between 220 s and 460 s, or between 3.7 and 7.7 min.

In accordance with the concept of a spherical global capacitor, Fig. 5 illustrates that the red conductivity $\sigma(h)$ curve and the black spherical capacitance line $C(h)$ intersect or touch each other at some altitude. This intersection defines the height of the capacitor which is sought. Obviously, this condition will be satisfied if the red curve is shifted slightly downward. We again note that σ_0 from Kudintseva et al. (2018) is smaller than the value that we have used here, by a factor of $\frac{1}{0.7586} = 1.318$. We can therefore multiply all the values in the Kudintseva et al. (2018) profile by this factor to bring the profile into near alignment with ours. This operation is equivalent to lowering the Kudintseva et al. (2016) profile by ~ 0.8 km. Such a lowered profile is presented in Fig. 6. The steps in the profile are the cause of the periodicity, with a vertical wavelength of 3 km that is evident in the scale height. Corresponding values of the capacitance, C, as given by equation (1), and conductivity at the upper plate, σ_b, are given in the columns on the right (2) of Table 1.

Using this profile, we obtain Fig. 7. The two curves in the left panel touch each other, or osculate, at a height of ~2 km, at the point of tangency. This is in the region of stratiform cloud tops where it is known that well defined positive charge layers exist (Nicoll and Harrison, 2016; Harrison et al., 2020). The median value of the positive charge density in these cloud-top layers is 43 pC/m^3.

We repeat in Fig. 7b the $C(h)$ plot already presented in Fig. 4b. These two panels of Fig. 7 support the visual evaluation of the effective capacitance of the global circuit. Using Table 1, we find that $C = 2.28$ F; the time constant is thus 456 s, or 7.6 min. This result is in very good agreement with the experimental determination of τ by Bór et al. (2023), to be between 7 and 8 min.

The profile suggested by Kudintseva et al. (2018) was originally constructed to fit both ELF electromagnetic and ULF electrostatic observational data. The present analysis indicates that this profile should be shifted downward by 0.8 km to fit the idea of the global electric circuit capacitance. We now show that such a modification does not violate its agreement with ELF observations, as there are no significant alterations to the Schumann resonance pattern. We take two σ(z) conductivity profiles in the 0–110 km range; one is the profile from Kudintseva et al. (2018) and the other is this profile shifted downward by 0.8 km. We calculate the parameters of ELF radio propagation for these profiles using the full wave solution in the form of the Riccati equation (see, e.g., Nickolaenko and Hayakawa, 2014; Kudintseva et al., 2016). Thus, we obtain the dispersion relations $\nu(f)$ relevant for both profiles. We then compute the two power spectra of the vertical electric field component in the Schumann resonance frequency band, with a uniform global distribution of lightning strokes. These spectra are found using the equation (see, e.g., Nickolaenko and Hayakawa, 2014, equation 5.15)

$$|E(f)|^2 = \left|\frac{\nu(\nu+1)}{2\pi f}\right|^2 \sum_{n=0}^{100} \frac{2n+1}{|n(n+1) - \nu(\nu+1)|^2} \tag{18}$$

With n being an integer, this formula is used for $\nu(f)$, with the original profile from Kudintseva et al. (2018) and the modified profile shifted down by 0.8 km. Shown in Fig. 8 are two computed power spectra of Schumann resonances for a uniform distribution of lightning strokes around the world. The black line corresponds to the conductivity profile 1, of Kudintseva et al. (2018), and the red line to the downward shifted profile 2. Both curves are practically coincident, which indicates that radio signals at Schumann resonance frequencies are insensitive to such a small alteration in atmospheric conductivity profile. The difference between these two profiles could result from calculations of conductivity profile taking into account the average land height level, a fairly recent estimate of which is 0.8 km (Eakins and Sharman, 2012).

Many published papers use model conductivity profiles for the stratosphere and mesosphere when addressing electric phenomena in

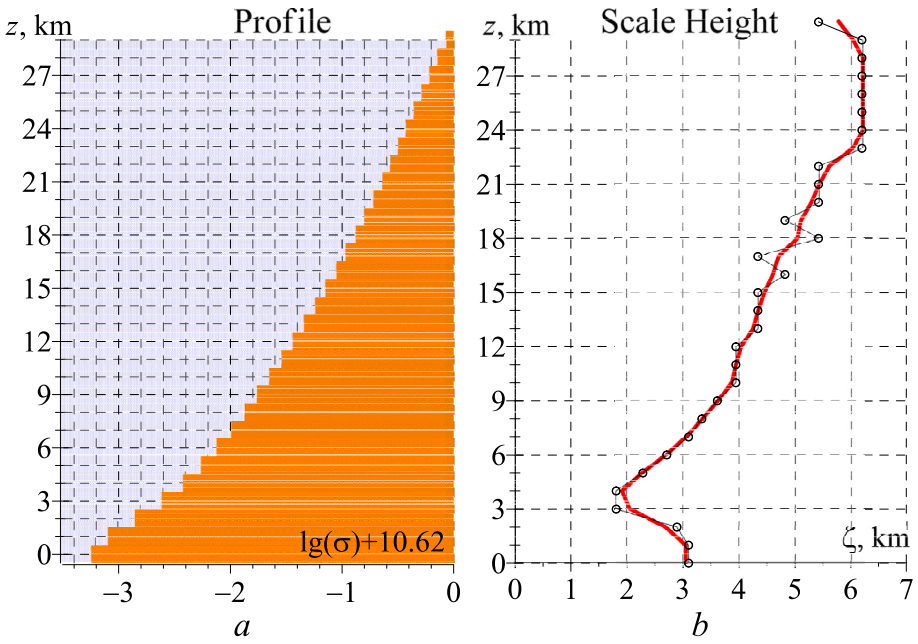

Fig. 6. a) Left. The height profile of the Kudintseva et al. (2018) conductivity, σ, in S/m, lowered by 0.8 km. b) Right. The corresponding scale height, ζ, variation, and smoothed (red curve).

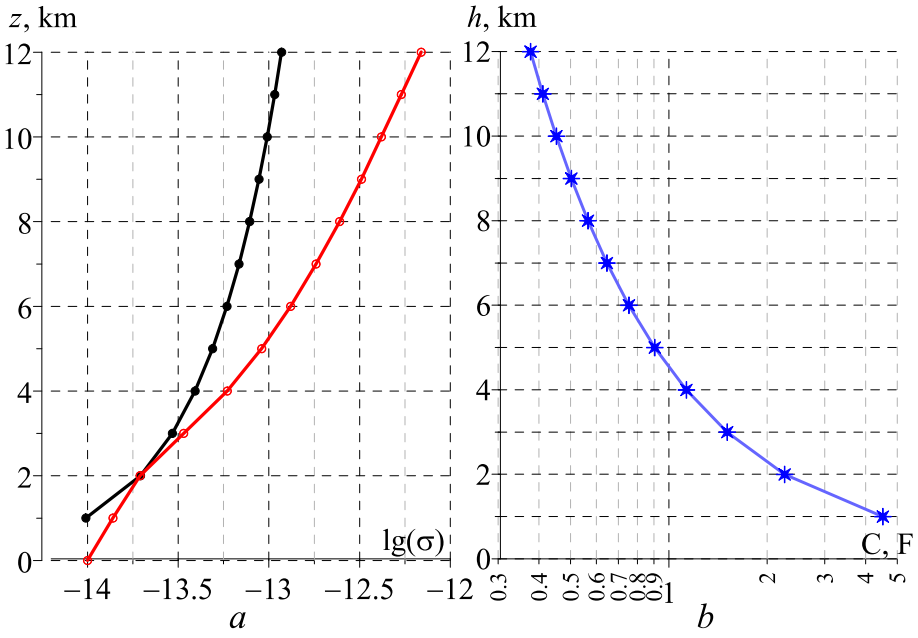

Fig. 7. a) Left. The black curve shows the capacitor height, h, plotted against $\lg(\sigma_b)$. The red curve shows the air conductivity profile of Kudintseva et al. (2018) lowered by 0.8 km. The two curves touch at a height of 2 km. b) Right. The relationship between the capacitance and the height of the capacitor's upper plate, the pseudo-electrode, from equation (1).

the ULF and VLF bands. We compare in Fig. 9 our profiles with a few typical profiles of atmospheric conductivity.

The purple line in Fig. 9a depicts the classic profile developed by Cole and Pierce (1965), which is widely used in VLF and ELF radio propagation studies. The black curve in this figure corresponds to the profile used by Denisenko et al. (2019a, b), which was developed specifically to describe the global electric circuit. The red and blue lines depict the profiles used in this paper.

The black line in Fig. 9a shows the Denisenko et al. (2019a, b) average profile, which itself combines a series of data in the literature that we show in Fig. 9b, reprinted from this publication. This figure shows the amount of data hidden behind many profiles published in the works of various authors. Line 1 is the profile of Rycroft and Odzimek (2010), line 2 corresponds to data from the Handbook of Geophysics, 1960 and line 3 presents the profile used by Molchanov and Hayakawa (2008) for earthquake-related investigations. The bold line in Fig. 9b is the average conductivity also shown by the black line in Fig. 9a. Fig. 9 demonstrates a remarkable closeness of all profiles in the height region below 30 km, which is the most influential region for estimating the effective capacitance and the time constant of the global electric circuit. Our model is therefore in close accord with generally accepted data. Only slight adjustments were required to obtain the estimates for the

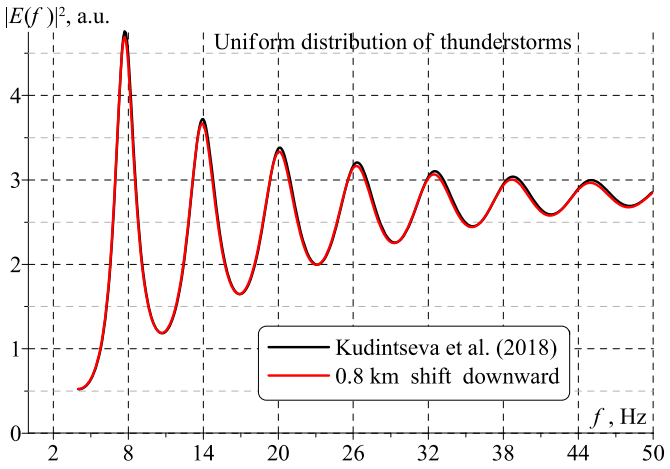

Fig. 8. Power spectra of Schumann resonances for uniform global distribution of lightning strokes in the Earth-ionosphere cavity, with the conductivity of air profile 1, from Kudintseva et al. (2018) (black curve), and that profile moved down by 0.8 km, profile 2 (red curve).

capacitance and the time constant of global electric circuit compatible with the recent 'direct' measurements during the explosive eruption of the Tonga-Haipai volcano (Bór et al., 2023).

At Schumann resonance frequencies, $f \sim 10$ Hz, using equation (17) gives

$$\sigma_b = 2\pi\varepsilon_0 \text{ x } 10 = 5.6 \text{ x } 10^{-10} \text{ S/m} \tag{19}$$

For the profile shown in Fig. 1 of Kudintseva et al. (2018), this occurs at a height of ~55 km; this is the characteristic electric height of Greifinger and Greifinger (1978). From Fig. 2 of Kudintseva et al. (2018), it is ~52 km by day and ~58 km at night. The characteristic magnetic height is almost twice this, ~97 km by day and ~102 km at night. The characteristic electric or magnetic heights are interpreted physically as the heights of the effective boundaries in the ionosphere above which the amplitude of the electric or magnetic field starts to rapidly decrease with increasing altitude when an upward propagating electromagnetic wave of frequency f is incident on the ionosphere. From Table 1, for a frequency of 1/456 Hz = 2.19 mHz, the characteristic electric height is 2 km and the characteristic magnetic height, where conduction currents flow, is ~140 km.

Greifinger and Greifinger (1978) showed that maximum Ohmic dissipation occurs at these characteristic heights. Madden and Thompson (1965) were the first to point out that "above about 50–60 km the conductivity term begins to dominate over the displacement current term" at Schumann resonance frequencies. Their Figs. 3 and 4 show that 7.5 Hz electromagnetic waves are highly damped, by day and by night, respectively, at heights of 50–60 km.

Fig. 10 plots the characteristic electric and magnetic heights as functions of frequency, f, in Hz, or period, $1/\omega$, in s, obtained from the full wave solution (Nickolaenko and Hayakawa, 2014) for a flat geometry, where the Earth's sphericity is ignored (Hynninen and Galuk, 1972; Bliokh et al., 1977; Jones and Knott, 1999). This is applicable at ELF, above 3 Hz; below this frequency, for ULF waves, the Earth's sphericity should be taken into account. Nonetheless, the characteristic electric height over the plane ground gives a qualitative result for the height of the global capacitor above the ground. Thus, Fig. 10 supports the results presented in this paper. However, the application of the characteristic magnetic height is problematic in this frequency range.

Combining equations (14) and (17), it is evident that the height of the pseudo-electrode, H, varies linearly with frequency, f. This is shown by the green line in Fig. 10 which starts at $f \sim 3$ mHz, period ~500 s, H ~2 km, the point of tangency shown in Fig. 7. This corresponds to values obtained using the profile presented in Fig. 6a.

5. Discussion in relation to GEC observations

One approach to determining τ from observations of the GEC is to select observations made at a time when there is a sudden change in the charging current that is distinguishable from the continuous charging by thunderstorms and electrified shower clouds occurring all around the world at all times. Such an opportunity is presented by the onset of significant volcanic lightning, see Van Eaton et al. (2023) and Shvets et al. (2024). To the best of our knowledge, we have only two occasions this century when atmospheric electricity observations were made at the Earth's surface during such an event, namely in Iceland in 2011 and in the Pacific in 2022. We consider the results presented by Rycroft et al. (2024) on the former, the Grímsvötn volcanic eruption, and by Bór et al. (2023) on the latter, the Hunga Tonga-Hunga Ha'apai eruption. For the former, τ was found to be between 7 and 12 min, peaking at 9 min, or 9 ± 3 min, and for the latter it was between 7 and 8 min. Both values agree

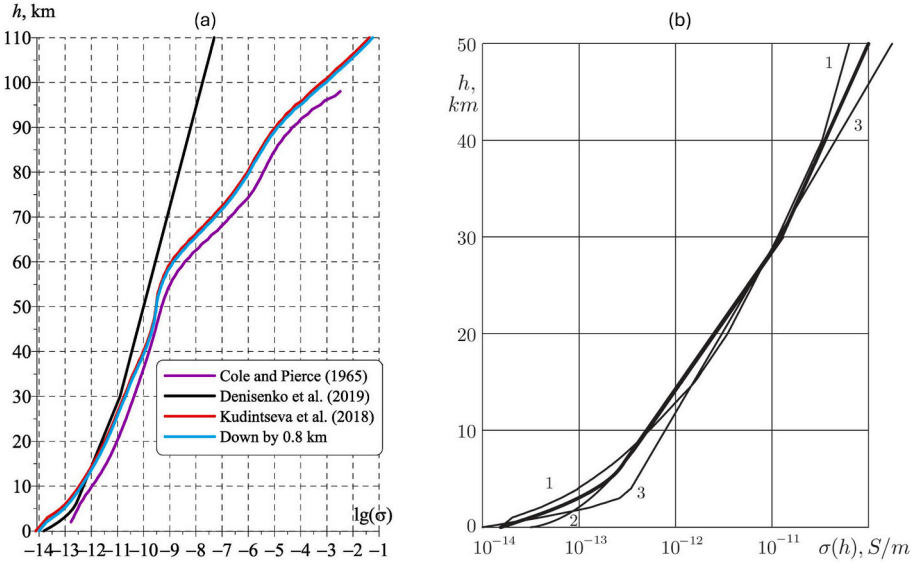

Fig. 9. Typical conductivity profiles of the troposphere, stratosphere and mesosphere used in the literature. a) Profiles considered in this paper. b) Profiles presented by Denisenko et al. (2019a, b), in their Fig. 4, and discussed in detail in the text.

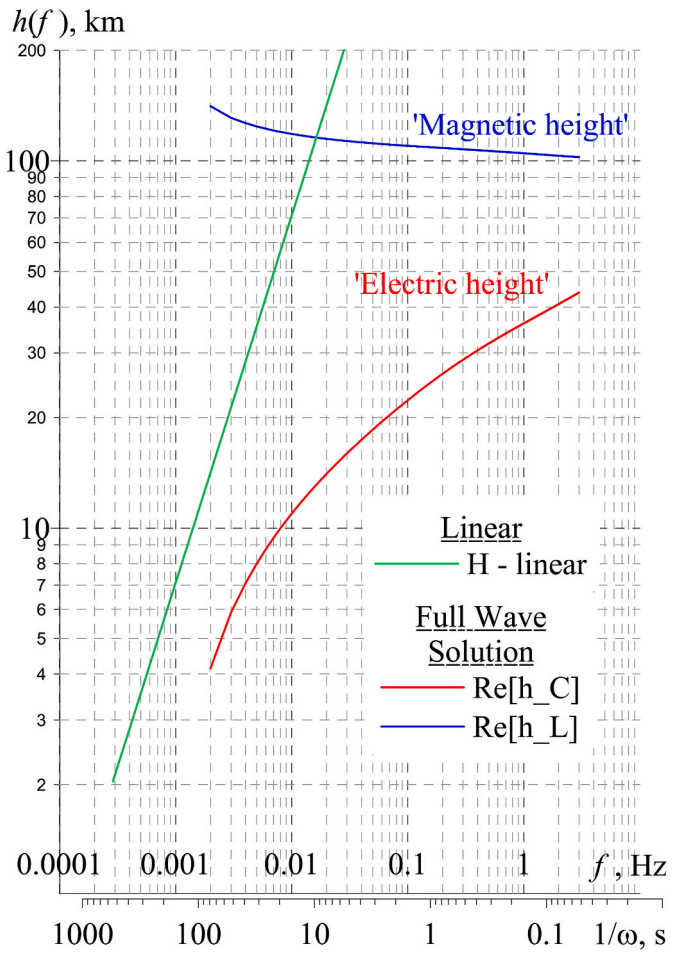

Fig. 10. The real part of the complex characteristic electric and magnetic heights of the conductivity profile are plotted against the ULF frequency and period. Also shown is the linear relation between H and f discussed in the text.

well with the theoretical value of 11 min, rounded from the 10.6 min given by equation (13).

However, it could be argued that the former value is larger than the latter value, which could possibly be explained by an ENSO effect on the GEC, first reported by Harrison et al. (2011). Slyunyaev et al. (2019, 2021a, b) investigated the links between the global circuit and the El Niño-Southern Oscillation (ENSO) (see also Sátori et al., 2009; Zheng et al., 2022). Harrison et al. (2022) demonstrated the presence of a relationship for most of the twentieth century between the vertical electric field observed at the surface at Lerwick, Shetland Islands, UK, and Watheroo, Australia, and ENSO. Subsequently Harrison and Riddick (2024) have demonstrated that from 1910 to 1950 such a relationship was also evident in measurements made at Eskdalemuir, UK.

Using the Oceanic Niño Index as a measure of the El Niño Southern Oscillation, Fig. 11 shows that both the May 2011 and the January 2022 events occurred close to the centre of periods of extended La Niña conditions. Thus, we cannot explain the slight difference in the time constant values for the two volcanic lightning events as being associated with different ENSO conditions, as might have been expected from the theoretical study of Slyunyaev et al. (2021a, b), see also Kozlov et al. (2023).

6. Links with life sciences

Without the smoothing effect characterised by the time constant, the electrical charging which results, e.g., at horizontal cloud and aerosol boundaries, could become transient or even non-existent. This is because

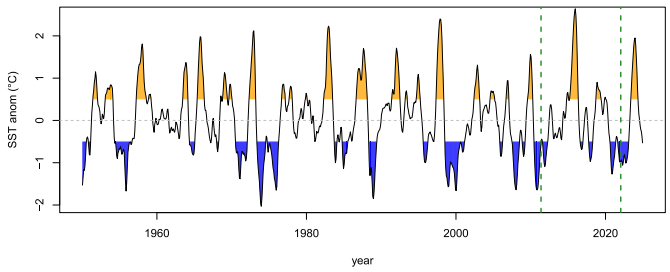

Fig. 11. Sea surface temperature (SST) anomalies from the Oceanic Niño Index, which is a three month running mean of SST anomalies in the Niño 3.4 region, are shown since 1950. Strong El Niño conditions are shown in orange, and the opposite, La Niña conditions, are shown in blue. 2011 and 2022 are marked with dashed lines, when the two volcanic lightning events being considered occurred.

the timescale of droplet growth is comparable or shorter than the GEC smoothing timescale. Most stratiform cloud droplet charging occurs in a narrow transition zone at the cloud base, estimated by Zhou and Tinsley (2012) to be only ~ 10 m. Hence, with updraft speeds of 0.1–1 m/s (Zheng et al., 2016, Fig. 2), the charging zone is encountered by growing droplets for ~10 s–100 s, which is typically shorter than the GEC relaxation timescale. This indicates that the steadiness of the background electrical conditions is likely to be a factor in facilitating the droplet charging.

Beyond these widespread physical processes having possible relevance to climate through influencing low-level clouds, there are biological situations in which the steadiness of the background electrical conditions from the GEC may also be important, such as providing electrostatic lift to ballooning spiders (Bell et al., 2005; Morley and Robert, 2018). Ballooning is the mechanism whereby spiders float away, e.g., from the top of a tree, when there is little wind, letting out silk as they go; this spreads out into the shape of a fan. Above the pointed leaves of the trees, which alter their surrounding electric fields (Hunting et al., 2021a), the electric field is enhanced, and so there is appreciable electrostatic force acting upwards on the spider's silk (Gorham, 2013). The physical and engineering properties of spider silk have recently been reviewed by Maithani et al. (2022); as has been known since the days of Faraday, it behaves as an electrical insulator. Thus, over some time, spiders can be propelled up to a stratus cloud and/or dispersed over appreciable horizontal distances, thereby aiding their migration.

Jackson et al. (2011) demonstrated that the behaviour of free-moving cockroaches is significantly influenced by static electric fields and that their responses are related to the field strength. Clarke et al. (2013, 2017) showed that bees, which are electrically charged, detect the electric fields around predominantly negatively charged flowers when they are pollinating them. Hunting et al. (2022) hypothesise that large aggregations of aerial insects provide an important source of space charge in the atmosphere. As an example of such an insect aggregation, they investigate a honeybee swarm because honeybees have a predictable swarming behaviour, and the existence of individual bee charges has been well documented. They provide model-based and empirical evidence that swarming, migrating bees make a contribution to the atmospheric electric field that depends on their density while they transport charge through the atmosphere.

England and Robert (2024) investigate electroreception, i.e. the ability of living creatures to perceive natural electrical stimuli, that enables prey species to detect predators using electrostatic fields. They show that predatory wasps are charged, and thus generate electric fields, and that caterpillars respond to such fields with defensive behaviours.

Hunting (2021) introduces research that links atmospheric electricity with biology and human well-being. Hunting et al. (2021b) have reviewed the connections between atmospheric electricity and biological systems. In addition to directly influencing biology, atmospheric electricity can have various indirect links to organisms and biological

processes.

Palmer et al. (2006) reviewed research on the effect of variations of geomagnetic activity on human cardiovascular health. Possible mechanisms by which space weather, i.e. variations in solar and geophysical parameters, could affect human health were discussed and the most likely candidates investigated. Stronger effects at higher latitudes seem to be observed. The direct effects of natural extremely low frequency electric and magnetic fields appear implausible; a mechanism involving some form of resonant absorption is more likely. The idea that the Schumann resonance signals could be the global environmental signal absorbed by the human body, thereby linking geomagnetic activity and human health was investigated. Mavromichalaki et al. (2021) have presented several statistical studies of the effects of solar, geomagnetic, and cosmic ray activity on human physiological parameters, such as heart rate and blood pressure. Very recently, Cui et al. (2024) have reported statistically significant beneficial effects of bursts of 20 Hz magnetic fields generated by coils adjacent to the heads of patients with treatment-resistant depression. Further research is required on how the properties of the GEC link into living systems which have evolved within the GEC.

7. Conclusions

The time constant of the GEC is the central parameter which characterises its damping response to the stochastic excitation of current pulses by conventional or volcanic lightning and by electrified storm systems. From this study, we conclude that.

(i) The exponential time constant, $\tau = RC$, of the global atmospheric electric circuit is approximately 10 min; this is consistent with both theoretical models and experimental observations. This means that, if all GEC current sources were to cease for 1 h, i.e. six time constants, the GEC would no longer exist.

(ii) The electrical properties of the air in the first few km of the atmosphere are much more influential in determining the properties of the DC global circuit than those at higher altitudes.

(iii) Stratus clouds over the oceans have a greater impact on the GEC time constant than do clouds over the land, due to the differences in air conductivity above the different surfaces caused by pollution over the land areas.

(iv) The concept of the Earth-ionosphere capacitor as an integral component of the DC GEC model is not valid. Nonetheless, it is definitely valid for the AC GEC model, and for the explanation of Schumann resonances as resonances of the Earth-ionosphere cavity.

(v) The Earth-atmosphere capacitor model, which we now term the *global circuit capacitor model*, suggests that the upper plate of the capacitor, the pseudo-electrode, is at an altitude of 1.8 km; this is significantly lower than the traditionally assumed scale height of the atmosphere, ~7 km. This new concept is valid for stratus clouds over ~30 % of the Earth's surface, with the remaining 70 % being cloud-free, where the GEC return current is flowing from the ionosphere through the atmosphere to ground.

(vi) The condition that the displacement current equals the conduction current leads to the pseudo-electrode being at a height of 2.0 km; this concept applies for electromagnetic waves with frequencies ~ 2 mHz. This is an important new result. The value of the global capacitor is 2.3 F (to two significant figures) so that the GEC has a time constant of 7.6 min, in agreement with the experimental results of Bór et al. (2023).

(vii) The best agreement with theory for both the DC and AC (Schumann resonances) GEC is obtained when the conductivity of the air profile published by Kudintseva et al. (2018) is moved down by 0.8 km; this corresponds to the mean elevation of the Earth's surface.

(viii) Sudden volcanic eruptions, such as the Grímsvötn eruption in 2011 and the Hunga Tonga-Hunga Ha'apai eruption in 2022, provide valuable data for studying changes in the GEC and for finding its time constant; the experimentally determined τ values of 9 ± 3 min agree well with those that are derived here from theoretical considerations. As these two events happened at the same phase of the ENSO cycle, the slight differences between them cannot be ascribed to an ENSO effect.

(ix) Investigations of the time relaxation of signals received at ground-level coming from low or upper atmosphere lightning need considerations of the inhomogeneity of the lowest portions of the fair weather atmosphere which, in the light of this research on the GEC, will have a considerable effect on these times.

(x) Some interesting relationships exist between atmospheric electricity and biology, involving spiders, bees, other insects and humans; further related studies which include the time constants of these systems are certainly needed.

CRediT authorship contribution statement

Michael J. Rycroft: Writing – review & editing, Writing – original draft, Methodology, Conceptualization. **Alexander P. Nickolaenko:** Writing – review & editing, Visualization, Validation, Software, Investigation, Data curation. **R. Giles Harrison:** Writing – review & editing, Conceptualization. **Anna Odzimek:** Writing – review & editing, Visualization, Validation, Software, Data curation, Conceptualization.

Declaration of competing interest

The authors declare that they have no known competing financial interests or personal relationships that could have appeared to influence the work reported in this paper.

Acknowledgements

The authors thank their many colleagues around the world for valuable discussions of the topics considered here over many years. They are also grateful to the two reviewers whose perceptive comments have improved this paper.

The data for Fig. 11 was provided by NOAA/CPC, via https://www.cpc.ncep.noaa.gov/data/indices/oni.ascii.txt.

A. Odzimek acknowledges support from a subsidy from the Ministry of Science and Higher Education to the Institute of Geophysics of the Polish Academy of Sciences.

Data availability

Data will be made available on request.

References

Baumgaertner, A.J.G., Thayer, J.P., Neely III, R.R., Lucas, G., 2013. Toward a comprehensive global electric circuit model: atmospheric conductivity and its variability in CESM1(WACCM) model simulations. J. Geophys. Res. Atmos. 118, 9221–9232. https://doi.org/10.1002/jgrd.50725.

Baumgaertner, A.J.G., Lucas, G.M., Thayer, J.P., Mallios, S.A., 2014. On the role of non-electric clouds in the global electric circuit. Atmos. Chem. Phys. Discuss. 14, 9815–9847. https://doi.org/10.5194/acpd-14-9815-2014.

Bell, J.R., Bohan, D.A., Shaw, E.M., Weyman, G.S., 2005. Ballooning dispersal using silk: world fauna, phylogenies, genetics and models. Bull. Entomol. Res. 95, 69–114. https://doi.org/10.1079/BER2004350.

Bliokh, P.V., Galuk, YuP., Hynninen, E.M., Nickolaenko, A.P., Rabinowicz, L.M., 1977. Resonance effects in the Earth-ionosphere cavity. Radiophys. Quantum Electron. 20 (4), 339–345. https://doi.org/10.1007/BF01033918.

Bór, J., Bozóki, T., Sátori, G., Williams, E., Behnke, S.A., Rycroft, M.J., Buzás, A., Silva, H.G., Kubicki, M., Said, R., Vagasky, C., Steinbach, P., Szabóné André, K., Atkinson, M., 2023. Responses of the AC/DC global electric circuit to volcanic electrical activity in the Hunga Tonga - hunga ha'apai eruption on 15 January 2022. J. Geophys. Res. Atmos. 128, e2022JD038238. https://doi.org/10.1029/2022JD038238.

Clarke, D., Whitney, H., Sutton, G., Robert, D., 2013. Detection and learning of floral electric fields by bumblebees. Science 340 (6128), 66–69. https://doi.org/10.1126/science.1230883.

Clarke, D., Morley, E., Robert, D., 2017. The bee, the flower, and the electric field: electric ecology and aerial electroreception. J. Comp. Physiol. 203, 737–748. https://doi.org/10.1007/s00359-017-1176-6.

Cole, R.K., Pierce, E.T., 1965. Electrification in the Earth's atmosphere from altitudes between 0 and 100 kilometers. J. Geophys. Res. 70 (11), 2735–2749, 1965.

Cui, H., Ding, H., Hu, L., Zhao, Y., Shu, Y., Voon, V., 2024. A novel dual-site OFC-dlPFC accelerated repetitive transcranial magnetic stimulation for depression: a pilot randomized controlled study. Psych. Med 1–14. https://doi.org/10.1017/S0033291724002289.

Denisenko, V.V., Rycroft, M.J., Harrison, R.G., 2019a. Mathematical simulation of the ionospheric electric field as a part of the Global Electric Circuit. Surv. Geophys. 40, 1–35. https://doi.org/10.1007/s10712-018-9499-6.

Denisenko, V.V., Rycroft, M.J., Harrison, R.G., 2019b. Correction to: mathematical simulation of the ionospheric electric field as a part of the global electric circuit. Surv. Geophys. 40, 37. https://doi.org/10.1007/s10712-018-9505-z.

Eakins, B.W., Sharman, G.F., 2012. Hypsographic Curve of Earth's Surface from ETOPO1. NOAA, National Geophysical Data Center, Boulder, CO.

England, S.J., Robert, D., 2024. Prey can detect predators via electroreception in air. Proc. Nat. Acad. Sci. 121 (23), e2322674121. https://doi.org/10.1073/pnas.2322674121.

Golubenko, K., Rozanov, E., Mironova, I., Karagodin, A., Usoskin, I., 2020. Natural sources of ionization and their impact on atmospheric electricity. Geophys. Res. Lett. 47, e2020GL088619. https://doi.org/10.1029/2020GL088619.

Gorham, P.W., 2013. Ballooning spiders: the case for electrostatic flight. arXiv, arXiv: 1309.4731v. http://arxiv.org/abs/1309.4731v.

Greifinger, C., Greifinger, P., 1978. Approximate method for determining ELF eigenvalues in the Earth-ionosphere waveguide. Radio Sci. 13, 831–837. https://doi.org/10.1029/RS013i005p00831.

Haldoupis, C., Rycroft, M., Williams, E., Price, C., 2017. Is the "Earth-ionosphere capacitor" a valid component in the atmospheric global electric circuit? J. Atmos. Sol. Terr. Phys. 164, 127–131. https://doi.org/10.1016/j.jastp.2017.08.012.

Handbook of Geophysics, 1960. United States Air Force. The Macmillan Company, New York.

Harrison, R.G., 2004. The global atmospheric electrical circuit and climate. Surv. Geophys. 25 (5–6), 441–484. https://doi.org/10.1007/s10712-004-5439-8.

Harrison, R.G., 2005. Columnar resistance changes in urban air. J. Atmos. Sol. Terr. Phys. 67, 763–773. https://doi.org/10.1016/j.jastp.2005.01.006.

Harrison, R.G., Joshi, M., Pascoe, K., 2011. Inferring convective responses to El Niño with atmospheric electricity measurements at Shetland. Environ. Res. Lett. 6, 044028. http://iopscience.iop.org/1748-9326/6/4/044028/.

Harrison, R.G., Marlton, G.J., Ambaum, M.H.P., Nicoll, K.A., 2022. Modifying natural droplet systems by charge injection. Phys. Rev. Res. 4, L022050. https://doi.org/10.1103/PhysRevResearch.4.L022050.

Harrison, R.G., Nicoll, K.A., Mareev, E., Slyunyaev, N., Rycroft, M.J., 2020. Extensive layer clouds in the global electric circuit: their effects on vertical charge distribution and storage. Proc. Roy. Soc. A 476, 20190758. https://doi.org/10.1098/rspa.2019.0758.

Harrison, R.G., Riddick, J.C., 2024. Atmospheric electricity observations at Eskdalemuir geophysical observatory. Hist. Geo Space Sci 15 (1), 5–16. https://doi.org/10.5194/hgss-15-5-2024.

Hunting, E.R., 2021. Atmospheric electricity: an underappreciated meteorological element governing biology and human well-being. Int. J. Biometeorol. 65, 1–3. https://doi.org/10.1007/s00484-020-02054-0.

Hunting, E.R., England, S.J., Robert, D., 2021a. Tree canopy influences ground level atmospheric electrical and biogeochemical variability. Front. Earth Sci. 9. https://doi.org/10.3389/feart.2021.671870.

Hunting, E.R., Matthews, J., de Arróyabe Hernáez, P.F., England, S.J., Kourtidis, K., Koh, K., Nicoll, K., Harrison, R.G., Manser, K., Price, C., Dragovic, S., Cifra, M., Odzimek, A., Robert, D., 2021b. Challenges in coupling atmospheric electricity with biological systems. Int. J. Biometeorol. 65, 45–58. https://doi.org/10.1007/s00484-020-01960-7.

Hunting, E.R., O'Reilly, L.J., Harrison, R.G., Manser, K., England, S.J., Harris, B.H., Robert, D., 2022. Observed electric charge of insect swarms and their contribution to atmospheric electricity. Science 25 (11), 105241. https://doi.org/10.1016/j.isci.2022.105241.

Hynninen, E.M., Galuk, YuP., 1972. Field of vertical electric dipole over spherical Earth with non-uniform along the height atmosphere. In: Problems of Diffraction and Radio Propagation, vol. 11. Leningrad University Press, Leningrad, pp. 100–120 (in Russian).

Ilin, N.V., Slyunyaev, N.N., Mareev, E.A., 2020. Toward a realistic representation of global electric circuit generators in models of atmospheric dynamics. J. Geophys. Res. Atmos. 125, e2019JD032130. https://doi.org/10.1029/2019JD032130.

Jackson, C.W., Hunt, E., Sharkh, S., Newland, P.L., 2011. Static electric fields modify the locomotory behaviour of cockroaches. J. Exp. Biol. 214, 2020–2026. https://doi.org/10.1242/jeb.053470.

Jánsky, J., Pasko, V.P., 2014. Charge balance and ionospheric potential dynamics in time-dependent global electric circuit model. J. Geophys. Res.-Space 119 (12), 10184–10203. https://doi.org/10.1002/2014JA020326.

Jones, D.L., Knott, M., 1999. Comparison of simplified and full-wave ELF propagation models. Abstracts of Reports at URSI General Assembly, Toronto, Session E6. August 1999.

Kamra, A.K., Murugavel, P., Pawar, S.D., Gopalakrishnan, V., 2001. Background aerosol concentration derived from the atmospheric electric conductivity measurements made over the Indian Ocean during INDOEX. J. Geophys. Res. 106, 28643–28652. https://doi.org/10.1029/2001JD900178.

Kamsali, N., Pawar, S.D., Murugavel, P., Gopalakrishnan, V., 2011. Estimation of small ion concentration near the Earth's surface. J. Atmos. Sol. Terr. Phys. 73 (16), 2345–2351. https://doi.org/10.1016/j.jastp.2011.07.011.

Kozlov, A.V., Slyunyaev, N.N., Ilin, N.V., Sarafanov, F.G., Frank-Kamenetsky, A.V., 2023. The effect of the madden-julian oscillation on the global electric circuit. Atmos. Res. 284, 106585. https://doi.org/10.1016/j.atmosres.2022.106585.

Kudintseva, I., Nickolaenko, A., Rycroft, M.J., Odzimek, A., 2016. AC and DC global electric circuit properties and the height profile of atmospheric conductivity. Ann. Geophys. Italy 59 (5), A0545. https://doi.org/10.4401/ag-6870.

Kudintseva, I.G., Galuk, Y.P., Nickolaenko, A.P., Hayakawa, M., 2018. Modifications of middle atmosphere conductivity during sudden ionospheric disturbances deduced from changes of Schumann resonance peak frequencies. Radio Sci. 53. https://doi.org/10.1029/2018RS006554.

Lavigne, T., Liu, C., Deierling, W., Mach, D., 2017. Relationship between the global electric circuit and electrified cloud parameters at diurnal, seasonal, and interannual timescales. J. Geophys. Res. Atmos. 122 (16), 8525–8542. https://doi.org/10.1002/2016JD026442.

Lucas, G.M., Baumgaertner, A.J.G., Thayer, J.P., 2015. A global electric circuit model within a community climate model. J. Geophys. Res. Atmos. 120 (23), 12054–12066. https://doi.org/10.1002/2015JD023562.

Madden, T., Thompson, W., 1965. Low-frequency electromagnetic oscillations of the earth-ionosphere cavity. Rev. Geophys. 3 (2), 211–254. https://doi.org/10.1029/RG003i002p00211.

Maithani, A., Sahni, I., Joshi, V.V., 2022. A review of thermal, physical, electrical properties of spider silk and their experimental setups. Mater. Today Proc. 62 (6), 3940–3949. https://doi.org/10.1016/j.matpr.2022.04.565.

Mareev, E.A., Volodin, E.M., 2014. Variation of the global electric circuit and Ionospheric potential in a general circulation model. Geophys. Res. Lett. 41, 9009–9016. https://doi.org/10.1002/2014GL062352.

Mavromichalaki, H., Papailiou, M.-C., Gerontidou, M., Dimitrova, S., Kudela, K., 2021. Human physiological parameters related to solar and geomagnetic disturbances: data from different geographic regions. Atmosphere 12 (12), 1613. https://doi.org/10.3390/atmos12121613.

Maynard, N.C. (Ed.), 1979. Middle Atmosphere Electrodynamics. Report of the Workshop on the Role of the Electrodynamics of the Middle Atmosphere on Solar Terrestrial Coupling, Reston, Virginia, January 17-19. Goddard Space Flight Center, Greenbelt, Maryland, NASA, p. 261.

Misaki, M., Ikegami, M., Kanazawa, I., 1972. Atmospheric electrical conductivity measurement in the Pacific Ocean, exploring the background level of global pollution. J. Meteorol. Soc. Japan 50 (5), 497–500.

Molchanov, O., Hayakawa, M., 2008. Seismo-Electromagnetics and Related Phenomena: History and Latest Results. TERRAPUB, Tokyo.

Morley, E.L., Robert, D., 2018. Electric fields elicit ballooning in spiders. Curr. Biol. 28 (14), 2324–2330.e2. https://doi.org/10.1016/j.cub.2018.05.057.

Nickolaenko, A., Hayakawa, M., 2014. Schumann Resonance for Tyros. Springer, Tokyo-Heidelberg-New York-Dordrecht-London, p. 348.

Nicoll, K.A., Harrison, R.G., 2016. Stratiform cloud electrification: comparison of theory with multiple in-cloud measurements. Q. J. R. Meteorol. Soc. 142, 2679–2691. https://doi.org/10.1002/qj.2858.

Palmer, S.J., Rycroft, M.J., Cermack, M., 2006. Solar and geomagnetic activity, extremely low frequency magnetic and electric fields and human health at the Earth's surface. Surv. Geophys. 27, 557–595. https://doi.org/10.1007/s10712-006-9010-7.

Potdar, S.S., Siingh, D., 2024. The atmospheric global electric circuit: a review. J. Ind. Geophys. Union 28 (4), 247–267.

Roble, R.G., Hays, P.B., 1979. Solar terrestrial coupling through atmospheric electricity. In: Middle, Atmosphere Electrodynamics, Maynard, N.C. (Eds.), Goddard Space Flight Center. NASA, Greenbelt, Maryland, pp. 89–139.

Rycroft, M.J., Israelsson, S., Price, C., 2000. The global atmospheric electric circuit, solar activity and climate change. J. Atmos. Sol. Terr. Phys. 62 (17–18), 1563–1576. https://doi.org/10.1016/S1364-6826(00)00112-7.

Rycroft, M.J., Odzimek, A., 2010. Effects of lightning and sprites on the ionospheric potential, and threshold effects on sprite initiation, obtained using an analog model of the global atmospheric electric circuit. J. Geophys. Res.-Space 115, A00E37. https://doi.org/10.1029/2009JA014758.

Rycroft, M.J., Odzimek, A., Arnold, N.F., Fullekrug, M., Kulak, A., Neubert, T., 2007. New model simulations of the global atmospheric electric circuit driven by thunderstorms and electrified shower clouds: the roles of lightning and sprites. J. Atmos. Sol. Terr. Phys. 69 (17–18), 2485–2509. https://doi.org/10.1016/j.jastp.2007.09.004.

Rycroft, M.J., Harrison, R.G., Nicoll, K.A., Mareev, E.A., 2008. An overview of earth's global electric circuit and atmospheric conductivity. Space Sci. Rev. 137, 83–105. https://doi.org/10.1007/s11214-008-9368-6.

Rycroft, M.J., Odzimek, A., Harrison, R.G., 2024. Determining the time constant of the global atmospheric electric circuit through modelling and observations. J. Atmos. Sol. Terr. Phys. 260, 106267. https://doi.org/10.1016/j.jastp.2024.106267.

Shvets, A.V., Hobara, Y., Hayakawa, M., Shvets, A.A., Koloskov, O., Yampolsky, Y., 2024. Investigation of anomalous lightning activity during the January 15, 2022 Tonga volcano eruption based on measurements of the VLF and ELF electromagnetic fields. J. Atmos. Sol. Terr. Phys. 264, 106344. https://doi.org/10.1016/j.jastp.2024.106344.

Sátori, G., Williams, E., Lemperger, I., 2009. Variability of global lightning activity on the ENSO time scale. Atmos. Res. 91 (2–4), 500–507. https://doi.org/10.1016/j.atmosres.2008.06.014.

Siingh, D., Gopalakrishnan, V., Singh, R.P., Kamra, A.K., Singh, S., Pant, V., Singh, R., Singh, A.K., 2007. The atmospheric global electric circuit: an overview. Atmos. Res. 84, 91–110. https://doi.org/10.1016/j.atmosres.2006.05.005.

Siingh, D., Singh, R.P., Jeni Victor, N., Kamra, A.K., 2023. The DC and AC global electric circuits and climate. Earth Sci. Rev. 244, 104542. https://doi.org/10.1016/j.earscirev.2023.104542.

Slyunyaev, N.N., Ilin, N.V., Mareev, E.A., 2019. Modeling contributions of continents and oceans to the diurnal variation of the global electric circuit. Geophys. Res. Lett. 46, 5516–5525. https://doi.org/10.1029/2019GL083166.

Slyunyaev, N.N., Frank-Kamenetsky, A.V., Ilin, N.V., Sarafanov, F.G., Shatalina, M.V., Mareev, E.A., Price, C.G., 2021a. Electric field measurements in the antarctic reveal patterns related to the El Niño-Southern Oscillation. Geophys. Res. Lett. 48 (21). https://doi.org/10.1029/2021GL095389.

Slyunyaev, N.N., Ilin, N.V., Mareev, E.A., Price, C.G., 2021b. A new link between El Niño-Southern Oscillation and atmospheric electricity. Environ. Res. Lett. 16 (4), 044025. https://doi.org/10.1088/1748-9326/abe908.

Tinsley, B.A., 2008. The global atmospheric electric circuit and its effects on cloud microphysics. Rep. Prog. Phys. 71 (66801), 31. https://doi.org/10.1088/0034-4885/71/6/066801.

Tinsley, B.A., 2022. Uncertainties in evaluating global electric circuit interactions with atmospheric clouds and aerosols, and consequences for radiation and dynamics. J. Geophys. Res. Atmos. 127, e2021JD035954. https://doi.org/10.1029/2021JD035954.

Tinsley, B.A., 2024. The influence of the solar wind electric and magnetic fields on the latitude and temporal variations of the current density, Jz, of the global electric circuit, with relevance to weather and climate. J. Atmos. Sol. Terr. Phys. 265, 106355. https://doi.org/10.1016/j.jastp.2024.106355.

Tinsley, B.A., Zhou, L., 2006. Initial results of a global circuit model with variable stratospheric and tropospheric aerosols. J. Geophys. Res. 111, D16205. https://doi.org/10.1029/2005JD006988.

Van Eaton, A.R., Lapierre, J., Behnke, S.A., Vagasky, C., Schultz, C.J., Pavolonis, M., Bedka, K., Khlopenkovet, K., 2023. Lightning rings and gravity waves: insights into the giant eruption plume from Tonga's Hunga Volcano on 15 January 2022. Geophys. Res. Lett. 50, e2022GL102341. https://doi.org/10.1029/2022GL102341.

Williams, E.R., 2009. The global electrical circuit: a review. Atmos. Res. 91 (2–4), 140–152.

Williams, E., Mareev, E., 2014. Recent progress on the global electrical circuit. Atmos. Res. 135–136, 208–227. https://doi.org/10.1016/j.atmosres.2013.05.015.

Wilson, C.T.R., 1903. Atmospheric electricity. Nature 68 (1753), 102–104. https://doi.org/10.1038/068102d0.

Wilson, C.T.R., 1906. On the measurements of the Earth-air current and on the origin of atmospheric electricity. Proc. Camb. Phil. Soc. 13, 363–382.

Wilson, C.T.R., 1921. Investigation on lightning discharges and on the electric field of thunderstorms. Phil. Trans. Roy. Soc. Lond. 211, 73–115. https://doi.org/10.1098/rsta.1921.0003.

Wilson, C.T.R., 1929. Some thunderstorm problems. J. Franklin Inst. 208, 1–12. https://doi.org/10.1016/S0016-0032(29)90935-2.

Zheng, F., Yuan, Y., Ding, Y., Li, K., Fang, X., Zhao, Y., Sun, Y., Zhu, J., Ke, Z., Wang, J., Jia, X., 2022. The 2020/21 extremely cold winter in China influenced by the synergistic effect of La Niña and warm Arctic. Adv. Atmos. Sci. 39 (4), 546–552. https://doi.org/10.1007/s00376-021-1033-y.

Zheng, Y., Rosenfeld, D., Li, Z., 2016. Quantifying cloud base updraft speeds of marine stratocumulus from cloud top radiative cooling. Geophys. Res. Lett. 43, 11407–11413. https://doi.org/10.1002/2016GL071185.

Zhou, L.M., Tinsley, B.A., 2010. Global circuit model with clouds. J. Atmos. Sci. 67, 1143–1156. https://doi.org/10.1175/2009JAS3208.1.

Zhou, L.M., Tinsley, B.A., 2012. Time dependent charging of layer clouds in the global electric circuit. Adv. Space Res. 50 (6), 828–842. https://doi.org/10.1016/j.asr.2011.12.018.